FIELD ANALYSIS TO OPTIMIZE CHARGE COLLECTION IN A SUB-MICRON GRATED METAL-SEMICONDUCTOR-METAL PHOTODETECTOR

S. Kache, N. S. Kranthi, M. O. Nizam, P. Kirawanich R. W. McLaren and N. E. Islam

Department of Electrical and Computer Engineering
University of Missouri-Columbia
Columbia, Missouri 65211, USA

A. K. Sharma, C. S. Mayberry, and S. L. Lucero

Air Force Research Laboratory
Space Vehicles Directorate
Kirtland AFB, New Mexico 87117, USA

Abstract—The effects of different geometries, heights and concentrations per unit area of gratings in the active region of a metal semiconductor metal photo-detector have been analyzed for enhanced charge collection through electromagnetic field analysis. Plots of the electric field amplitude as it propagates from the constricted grating region to a larger cross-section in the active region have been studied for comparison. This study shows that a hatched top cone shaped grating allows for maximum energy transfer into the active region, thus enhancing collection. The height for this structure is also a minimum over all structures, thus making the hatched cone the optimum design for enhanced collection. The cladding of such structures with SiO_2 also appears to contribute to increased energy transfer into the substrate.

1. INTRODUCTION

A photodetector (PD) is an important component of an optical transmission and receiver system. For fast and reliable operations, such systems require detectors with high efficiency, good responsivity and wide bandwidth. A class of devices known as metal-semiconductor-metal (MSM) photodetectors meets these requirements and has been

widely used in many optical and measurement systems [1]. MSM PD is a planar device with Schottky barriers on either side of an exposed semiconductor absorption region. It requires low fabrication processing steps and has high speed because of low capacitance. The electrodes in these devices are often interdigitated to increase the active region area while optimizing the electric fields in the carrier collection region.

Because of its weak absorption at laser wavelengths as compared to GaAs and also due to its indirect bandgap characteristics, a Si MSM detector is unable to deliver acceptable ranges of efficiency and speed as its compared to its GaAs counterpart. GaAs PD's are currently used in many applications but are difficult to integrate with the existing Si chips, which leads to high costs in production. A well designed Si MSM photodetector is still an attractive choice in many applications including the next generation of high performance optical communication interconnects [2]. In addition; Si MSMs are compatible with the VLSI technology [3].

In recent years, many attempts have been made to improve the quantum efficiency of Si MSM detectors. These attempts include etching deep vertical and U-shaped trench electrodes, where the devices have shown improvement compared to planar contact devices [4-5]. The process is expensive and leads to fabrication difficulties. Detectors fabricated using SOI technology have enhanced speed, which is essentially due to the buried oxide layer which limits Si thickness [6]. Amorphous Si can be used to increase absorption, in cases where the focus is to modify the long-range structural symmetry of crystalline Si, thereby relaxing the k-vector selection rule for optical transitions [7]. This method reduces the efficiency and also has problems with integration with Si chips. Finally, in an attempt to improve absorption in the active region, a 1000-nm deep sub-wavelength grating is integrated on the top of the active region of the Si MSM structure. This results in an increased collection of charge [8]. The physics for the improved collection, however, has not been fully explained.

One plausible explanation for improved collection has been recently presented using electromagnetic (EM) field analysis [9]. Here, it was shown that charge collection in an MSM photo detector can be studied by tracing the amplitude of the transmitted E-field into the active region of the detector. An increase in the transmitted E-field amplitude means an increase in the transmission coefficient, $(\tau = \frac{E_0^t}{E_0^i})$. The transmission coefficient then determines the energy carried by the transmitted wave $(S_{AV} = |\tau|^2 \frac{|E_0^i|^2}{2\eta})$ into the detector's active region. Field analysis also showed that charge collection can

be further increased by rearranging the wall-like grating lattice into a square shaped configuration.

In this paper, the EM field transport process is investigated further. In particular, a detailed analysis of the grating structure is performed in order to optimize charge collection. The grating geometry, height and concentration per unit active area are investigated for maximum energy deposition in the active region. The variation in the transmitted electric field energy that is deposited in the active region as a function of grating geometry was determined and analyzed to ensure the maximum possible collection. Finally, this paper also analyzes the effects of coating over these grating structures to examine the variations in the electric field in the substrate (active region). Section 2 provides a brief description of the simulation setup and theory. In Section 3 results and discussions are provided for this analysis and conclusions are presented in Section 4.

2. THEORY AND SIMULATION SETUP

The basic concept of a greater transmission of EM energy in the active region due to gratings on the surface has been presented earlier and is therefore not the subject of analysis here. It was shown previously that an amplitude variation occurs when an EM wave enters the detector's active region while traveling through the gratings - a region of different cross-sectional area [9]. A higher transmission coefficient translates to more transmitted energy into the active region. Hence, the concept of increasing the transmission energy by allowing the electromagnetic waves to pass through gratings with varying geometry, and concentration on the active region can be used to design structures that optimize collection.

The simulation method used in this study is based on the Finite Integration Technique (FIT), which provides a discrete reformulation of Maxwell's equations in their integral form suitable for computers applied to electromagnetic field problems with complex geometries. The associated integral form of a grid cell surface can be written as the differential equation

$$e_x(i,j,k) + e_y(i,+1,i,k) - e_x(i,j+1,k) - e_y(i,j,k) = -\frac{d}{dt}b_z(i,j,k), \tag{1}$$

where the scalar value $e_x(i,j,k) = \int_{(x_i,y_j,z_k)}^{(x_{i+1},y_j,z_k)} \vec{E} \cdot d\vec{s}$ represents the exact value of the integral over the distance limits of the electric field, and the scalar value $b_z(i,j,k) = \int_{A_Z(i,j,k)} \vec{B} \cdot d\vec{A}$ represents the integral over the area of the magnetic flux density. Simulation equations using
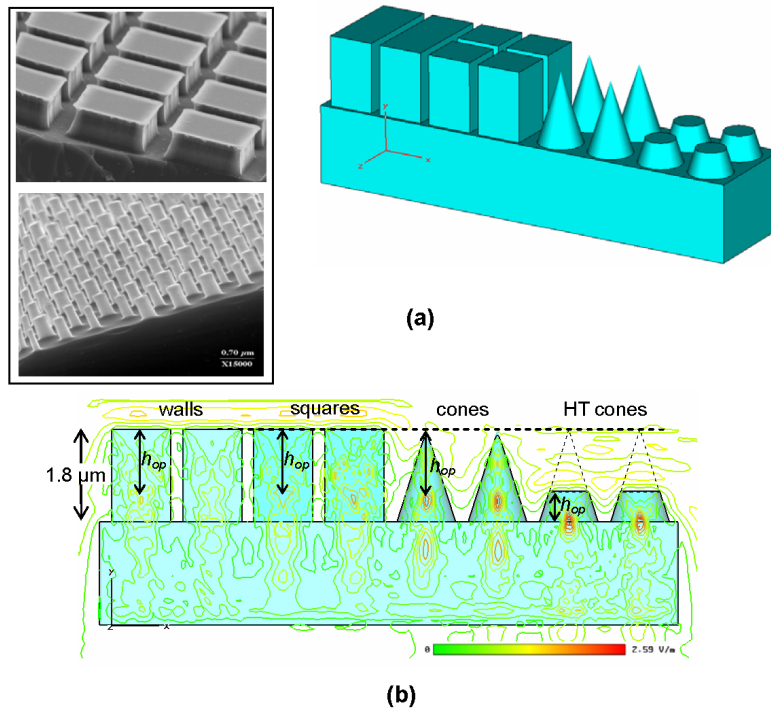
Figure 1. (a) Bulk Si detector with different 1.8-μm tall grating structures, i.e., wall, square, cone, and hatched-top cone. The inset shows SEP pictures of nano gratings that were fabricated by AFRL, for possible placement on the active region. (b) Maximum isoline plot of the incident wave transmitted through substrate, square, cone, and hatched-top cone structures. The curves display the optimum height, h_{op}, of each structure.

this technique are incorporated in a commercial code that has been used in this analysis [10].

The simulation scheme is shown in Fig. 1a. In this setup, a section of the detector with four grating structures (wall, square, cone, and hatched-top cone, two of the structures fabricated through interferometric lithography are shown in the inset), each 1.8-μm in height, are to be simulated and compared for analysis. The transmission of a z-polarized incident wave through the structures will generate changes in the wave amplitude as it crosses the region into the active area. The plots generated through simulations will be compared
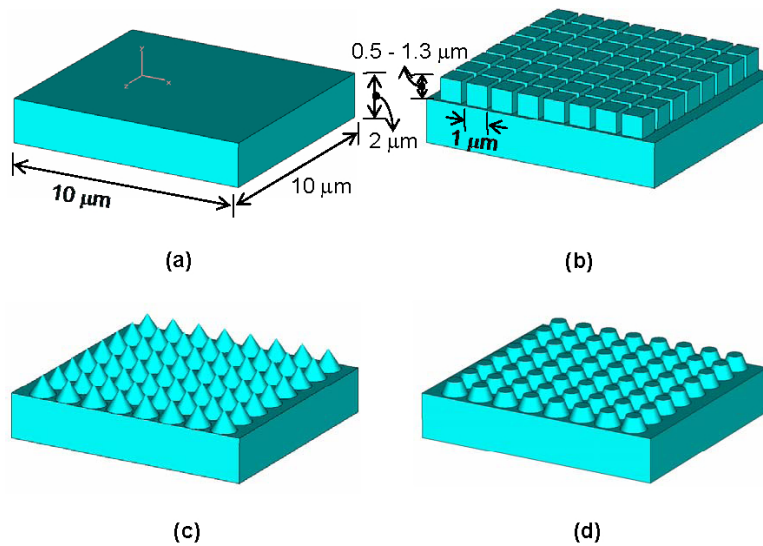
Figure 2. Configurations of MSM photodetectors used in the simulations. Structures are a $10 \times 10 \times 2\,\mu$m Si-substrate (a) without gratings, (b) square gratings, (c) cone gratings, and (d) hatched-top cone gratings.

in the analysis, first to determine the best structure shape that will allow for maximum energy transmission and later, after the shape is determined, its height will be optimized. Fig. 1b shows a maximum isoline plot of the four best shapes in the 2D plane. It shows that the hatched-top cone has the highest E-field amplitude close to the active region while the wall-type grating has the lowest maximum peak. This suggests that grating structures such as a square, cone, and hatched-top cone have similar effects as that of a wall-like grating (inset Fig. 1a) structure, and will contribute towards enhancing charge collection as was demonstrated earlier [9].

For simulations, a $10 \times 10 \times 2\,\mu$m Si region, representing a section of the detector's active region, was used in the simulations as shown in Fig. 2a. A $1\,$V/m plane wave port as the source in the negative y-direction with a continuous sinusoidal wave was also used as the excitation signal. It is also important to note that diffraction theory and absorption through gratings will not explain all the physics associated with charge collection. For Si, the incident wave must have energy equal to or greater than the material bandgap and hence would be capable of creating electron-hole pairs at the interface

[15]. Therefore, in this study, a wave length corresponding to the bandgap energy was chosen for the incident plane wave. In order to optimize the grating shape for maximum transmission, different geometries (i.e., square, cone and hatched-top cone), were chosen for comparison as shown in Figs. 2b, 2c, and 2d. E-fields were monitored by placing probes at the interface between the grating and the Si substrate. Due to changes in structural shape and the effects of refraction and transmission there is a change in the transmission coefficient (transmitted energy) as the E-field passes from one region to another. Simulation results to optimize the transmitted energy are discussed in Subsections 3.1, 3.2, and 3.3. Results from SiO_2 cladding on the gratings is also included in the discussion.

3. RESULTS AND DISCUSSIONS

3.1. Optimization by Varying the Height of the Gratings

Structures shown in Fig. 2 were simulated by varying the height of the gratings in the 0.5–1.3 μm range, while the area covered on the active region was kept the same for all the structures. The plots of normalized E-field amplitudes associated with the square, cone, and hatched-top cone structures with different heights are shown in the Fig. 3. One can see that each structure has a unique optimum height, hop, with the square, cone, and hatched-top cone having the optimum heights of 1.0 μm, 0.9 μm, and 0.6 μm, respectively. The hatched-top cone structure of Fig. 2d shows a maximum normalized amplitude of 2.45 V at a height of 0.6 μm as shown in Fig. 4. Since transmitted amplitude contributes to the transmission coefficient (which effects transmitted power), this structure therefore allows for maximum energy transfer into the substrate. The fabrication cost is also expected to be the least for this structure due to its low height, h_{op}.

A geometrical analysis of the focal point for the E-field of the hatched-top cone is shown in Fig. 5a and is based on concepts presented elsewhere [12]. This structure can be decomposed into cylindrical and hollow-center hatched-top cone components. For the cylindrical component, the z-polarized wave transmits from air through Si with a transmission coefficient of τ_{OA}. For the hollow-center hatched-top cone component, the oblique incident wave makes an angle of θ_1 and the transmitted wave makes an angle of θ_2 with respect to the normal axis to the surface. In this case, a constructive interference of E-fields could be attributed to the increase in the E-field. Other structures will not have this trend. The circular distribution of associated transmission coefficients on this component is illustrated in detail in Fig. 5b. The figure depicts the top view in the xz plane. The entire Si area can
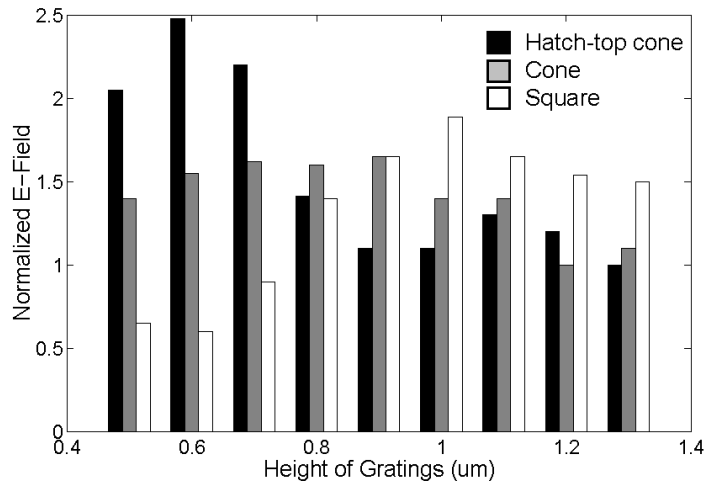
Figure 3. Normalized (with $1\,\mathrm{V/m}$) E-field peak associated with square (white), cone (gray), and hatched-top cone (black) structures as a function of height.
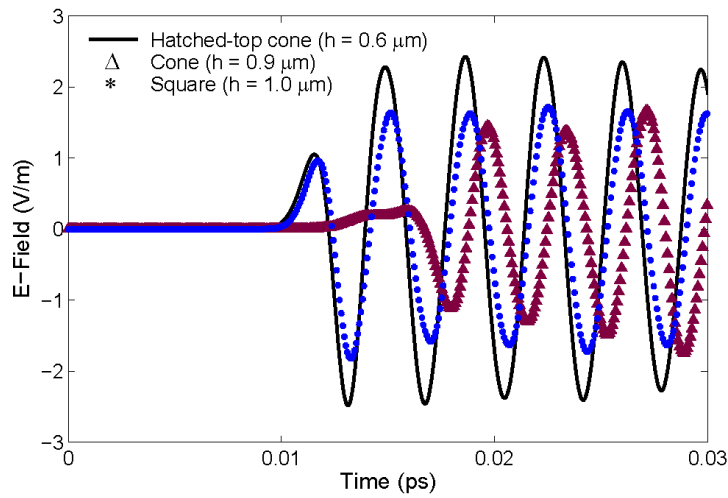
Figure 4. E-field vs. time waveforms of three structures associated with their optimum heights. (solid line: hatched-top cone with height $= 0.6\,\mu\mathrm{m}$, triangles: cone with height $= 0.9\,\mu\mathrm{m}$, and asterisks: square with height $= 1\,\mu\mathrm{m}$).
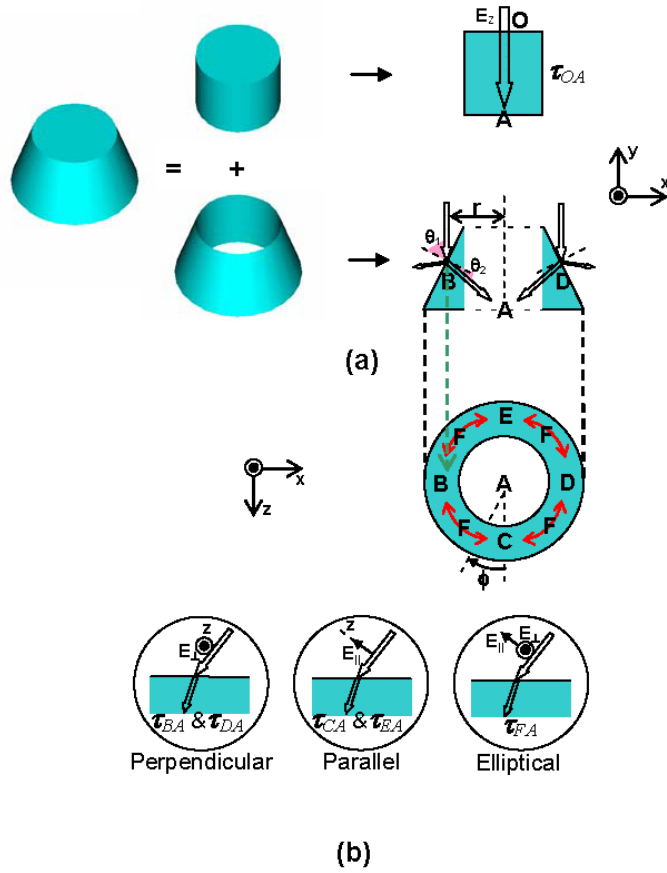
Figure 5. Decomposition of the hatched-top cone grating: (a) side view of decomposed cylindrical and hollow-center hatched-top cone components on xy plane and (b) top view of the hollow-center hatched-top cone components on xz plane.

be divided into five regions, i.e., B, C, D, E, and F. At locations C and E, the electric fields are parallel polarized while the electric fields at locations B and D are perpendicularly polarized. The transmission coefficients of the waves transmitting to locations A are τ_{CA} and τ_{EA} for the former case, and τ_{BA} and τ_{DA} for the latter case. The special case corresponds to locations within the region labeled F is of the elliptical polarization. The transmission coefficient τ_{FA} is determined by an integral over this region of individual transmission coefficients

associated with different elliptically polarized incident waves. The total transmission coefficient can be determined from the contributions from individual components and is expressed as

$$\tau_\Sigma = \tau_{OA} + \sum_{\phi=0}^{2\pi} \tau_\phi, \tag{2}$$

where the summation term on the right hand side represents an integration of transmission coefficients between locations B to F (Fig. 5b). The contribution of these components enhances the transmitted energy, and the transmitted electric field in Si can now be written as

$$\boldsymbol{E}_t = \tau_\Sigma \cdot E_0 e^{j(\omega t - \beta y)} \hat{\boldsymbol{z}}, \tag{3}$$

where E_0 is the incident wave amplitude and β is the phase constant.

In the cases of a wall, a square and a cone, the focal point is not close to the active region. Also, as the height is increased, the focal point shifts slightly towards the top, and thus, there is a decrease in the E-field. Thus, the large transmitted amplitude for the hatched-top cone as compared to the other two structures could be due to a combination of the effects of slanted-sides and flat-top surfaces that result in focusing the transmitted waves on one particular spot close to the top surface. As a result, the hatched-top cone structure has high E-fields. Further analysis in this paper is therefore dedicated to the hatched-top cone structure.

3.2. Optimization by Varying Number of Gratings on the Active Region

The number of grating structures on the active region was varied to optimize the charge collection. This effectively changed the area covered by the gratings while keeping the area of the active region constant that is the percentage of area covered by the Si gratings on the active region changes. The dimension of each grating structure is kept constant at $a\,\mu\mathrm{m}^2$ where a is the area covered by each grating structure on the active region. Hence, the entire area covered by the gratings is $na\,\mu\mathrm{m}^2$ (n = number of gratings).

The relationship between the number of gratings and the normalized E-field peak for the hatched-top cone structure is shown in Fig. 6. The maximum E-field corresponds to 100 hatched-top gratings. The E-field magnitude starts at a low value and then slowly increases until a critical number of gratings is reached and then starts to decrease. This is because, a smaller number of gratings, the distance between the structures is larger than the wavelength
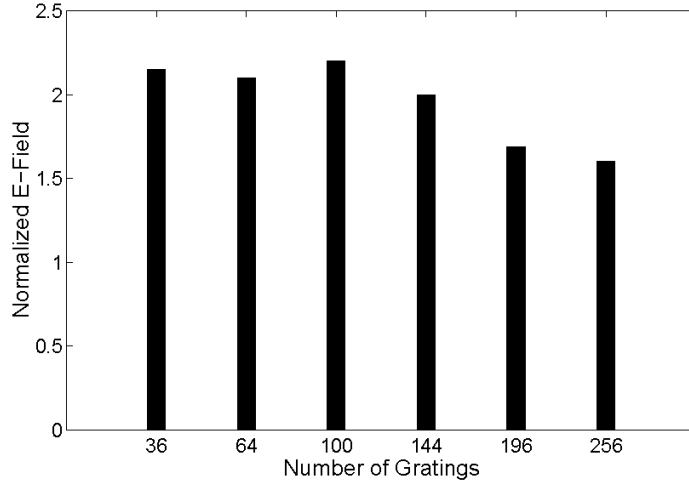
Figure 6. Relationship between the number of gratings and the normalized E-field peak for the structure with hatched-top cone gratings.

and there is no contribution from adjacent regions. As the number of gratings increases, the separation distance between the gratings decreases which causes multiple constructive interference similar to the situation described earlier. This causes the E-field magnitude to increase. As the number of gratings increases further, the E field starts to decrease. The reason is that the large number of clusters makes the region behave as a bulk region [13, 14].

3.3. Optimization of the Charge Collection by Using a Cladding of SiO$_2$

Finally, changes in the transmitted E-field magnitude were studied with SiO$_2$ layers on the grating surface. Oxides grow naturally on exposed Si surfaces primarily due to the interaction of Si dangling bonds with oxygen in air. Most practical devices are expected to have such a layer. A hatched-top cone grating, which generated the optimum E-field amplitude in the active region, was used in the simulation (Fig. 7). The oxide thickness on the grating surface was about $0.05\,\mu$m. Again, the E-field probe was placed at the interface between Si in the active region and the gratings. A comparison of Fig. 4 and Fig. 8 shows that there is no significant difference in the
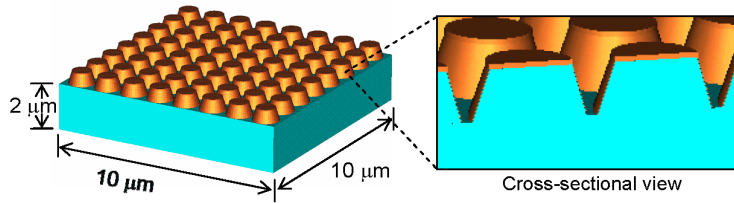
Figure 7. Structure consisting of a $10 \times 10 \times 2\,\mu$m Si substrate. The Si hatched-top cone gratings on top of the bulk SiO_2 are coated with a SiO_2 layer of $0.1\,\mu$m thickness.
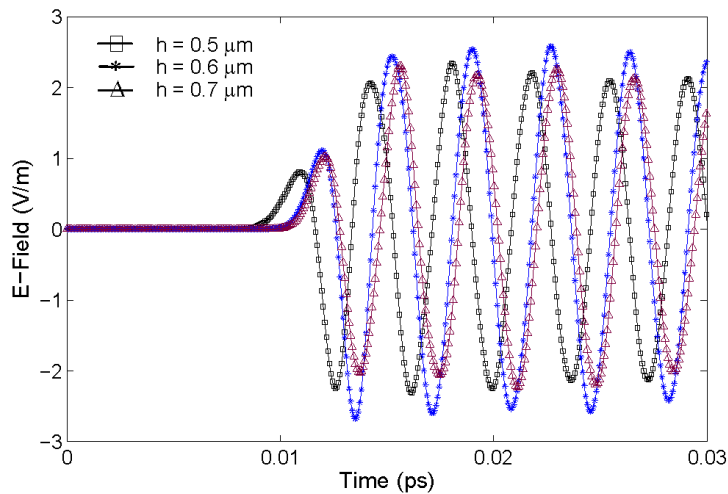
Figure 8. Waveforms of E-fields of a structure consisting of hatched-top cones of Si and an SiO_2 coating with different heights (squares: $0.5\,\mu$m, asterisks: $0.6\,\mu$m, and triangles: $0.7\,\mu$m).

E-field amplitude with the oxide layer on top of the optimum height ($0.6\,\mu$m, hatched-top cone structure). In order to determine a new optimum height, the structure height was then altered to values of 0.5 and $0.7\,\mu$m. No significant change in transmitted E-field amplitude was seen. However, improvements in transmission amplitude occur when the grating thickness is increased to a quarter wavelength. This is shown in Fig. 9. The quarter wavelength thickness is expected to minimize reflection at the interface through destructive interference.
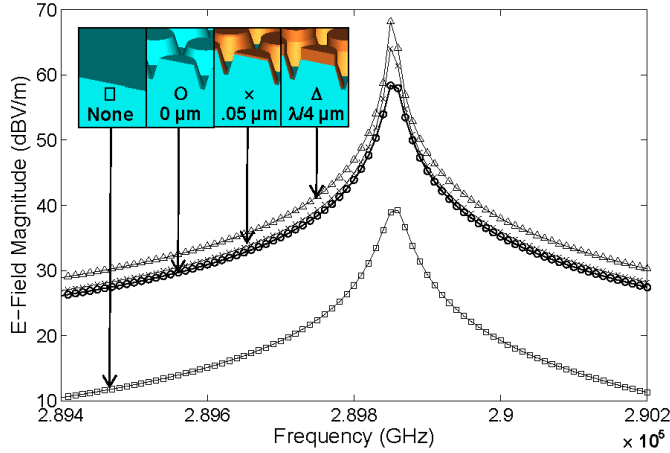
Figure 9. *E*-field magnitude frequency components (dBV/m) associated with the substrate without gratings (Squares) and the substrate with three cladding thickness cases (Circles: $0\,\mu$m, Crosses: $0.05\,\mu$m, and Triangles: $0.258\,\mu$m).

4. CONCLUSION

Charge collection in a MSM photo detector can be studied by tracing the amplitude of the transmitted *E*-field into the active region of the detector. An increase in the transmitted *E*-field amplitude means an increase in the transmission coefficient. The transmission coefficient determines the energy carried by the transmitted wave into the detector's active region. Simulations show that collection in MSM detectors can be improved by adding gratings in the active region. Simulations also show that the energy deposited in the active region depends on the shape and height of the gratings. This indirectly affects the charge collection of the photodetector.

A comparison of three different shapes show that a cone shaped grating with a hatched-top is the best structure for enhancing collection. The distance between gratings also affects the overall collection. Also a cladding around the gratings can be used to improve the collection further. The hatched-top cone grating with a quarter wave length of SiO_2 as cladding has shown the best results. It is postulated that the charge collection can be improved further in MSM photodetectors by using a different grating shape or by improvising on the material used for cladding.

REFERENCES

1. Nalwa, H. S., *Photodetectors and Fiber Optics*, Academic Press, 2001.

2. Chou, S. Y. and M. Y. Liu, "Nanoscale tera-hertz metal-semiconductor-metal photodetectors," *IEEE J. Quantum Electron.*, Vol. 28, 2358–2368, 1992.

3. Mullins, B. W., S. F. Soares, K. A. McArdle, C. Wilson, and S. R. J. Brueck, "A simple high-speed Si Schottky photodiode," *IEEE Photon. Technol. Lett.*, Vol. 3, 360–362, 1991.

4. Ho, Y. L. and K. S. Wong, "Bandwidth enhancement in silicon metal-semiconductor-metal photodetector by trench formation," *IEEE Photon. Technol. Lett.*, Vol. 8, 1064–1066, 1996.

5. Laih, L.-H., T.-C. Chang, Y.-A. Chen, W.-C. Tsay, and J.-W. Hong, "Characteristics of MSM photodetectors with trench electrodes on p-type Si wafer," *IEEE Trans. Electron Devices*, Vol. 45, 2018–2023, 1998.

6. Liu, M. Y., E. Chen, and S. Y. Chou, "140-GHz metal-semiconductor-metal photodetectors on silicon-on-insulator substrate with a scaled active layer," *Appl. Phys. Lett.*, Vol. 65, 887–888, 1994.

7. Mott, N. F. and E. A. Davis, *Electronic Processes in Noncrystalline Materials*, 2nd ed., Oxford Univ. Press, Oxford, U.K., 1979.

8. Sharma, A. K., S. H.Zaidi, P. C. Logofatu, and S. R. J. Brueck, "Optical and electrical properties of nanostructured metal-silicon-metal photodetectors," *IEEE J. Quantum Electron.*, Vol. 38, 1651–1660, 2002.

9. Kranthi, N. S., M. O. Nizam, P. Kirawanich, N. E. Islam, A. K. Sharma, and S. L. Lucero, "Fields analysis of enhanced charge collection in nanoscale grated photo detectors," *Appl. Phys. Lett.*, Vol. 87, 244101, 2005.

10. CST Microwave Studio 5.0, Sonnet Software, Inc., *User Manual*, 2005.

11. Sharma, A. K., S. H. Zaidi, G. Liecthy, and S. R. J. Brueck, "Enhanced optical and electrical characteristics of Si detectors integrated with periodic 1-D and 2-D semiconductor nanoscale structures," *Proc. IEEE Nanotechnology, 2001*, 368–373, 2001.

12. Kraus, J. D. and D. A. Fleisch, *Electromagnetics with Applications*, 5th ed., McGraw-Hill Companies, Inc., Singapore, 1999.

13. Kristensson, G., "Homogenization of corrugated interfaces in electromagnetics," *Progress in Electromagnetic Research*, PIER 55, 1–31, 2005.

14. Gaylord, T. K. and M. G. Moharam, "Analysis and applications of optical diffraction by gratings," *IEEE Trans. Electron Devices*, Vol. 73, 894–937, 1985.

15. Sze, S. M., *Physics of Semiconductor Devices*, 2nd ed., John Wiley & Sons, Inc., New York, 1981.